Electronic Supplementary Material (ESI) for Journal of Materials Chemistry C.
This journal is © The Royal Society of Chemistry 2015

Supporting Information

Production of centimeter-scale sub-wavelength nanopatterns by controlling the light path of adhesive photomask

Jin Wu[a], Kai Tao[a] and Jianmin Miao*[a]

[a]School of Mechanical and Aerospace Engineering, Nanyang Technological University, 50 Nanyang Avenue, Singapore 639798.

Email: MJMMiao@ntu.edu.sg

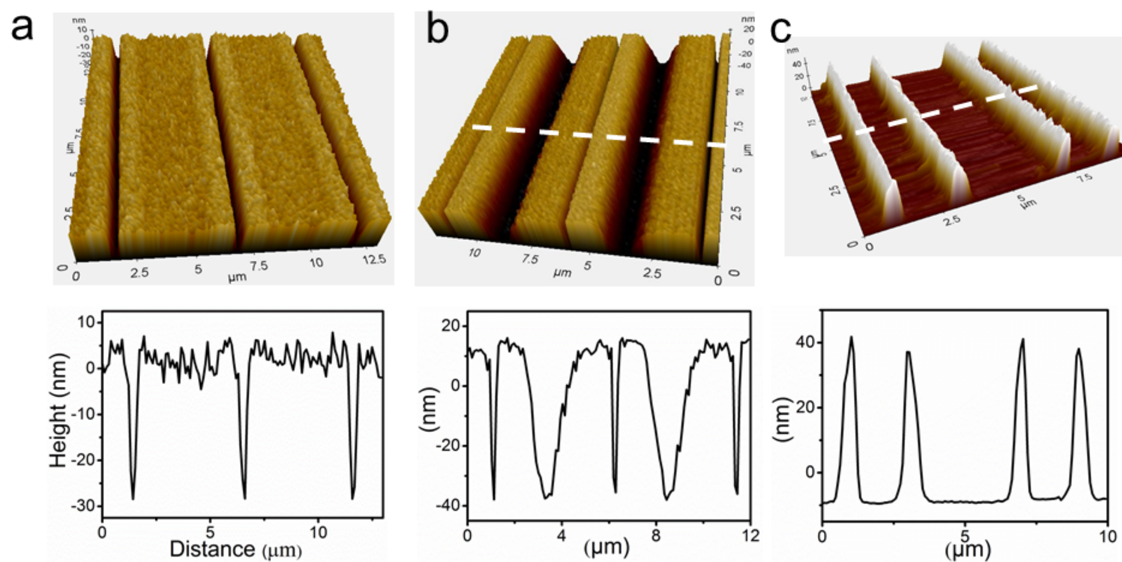

Figure S1. Investigation of the influence of exposure dose on the morphology of produced positive photoresist structures by exploiting 20 nm Au coated V-shape PDMS tip array as photomask. (a, b and c) 3D AFM topographical images of positive photoresist nanostructures produced using the exposure time of 2, 10 and 15 s respectively.

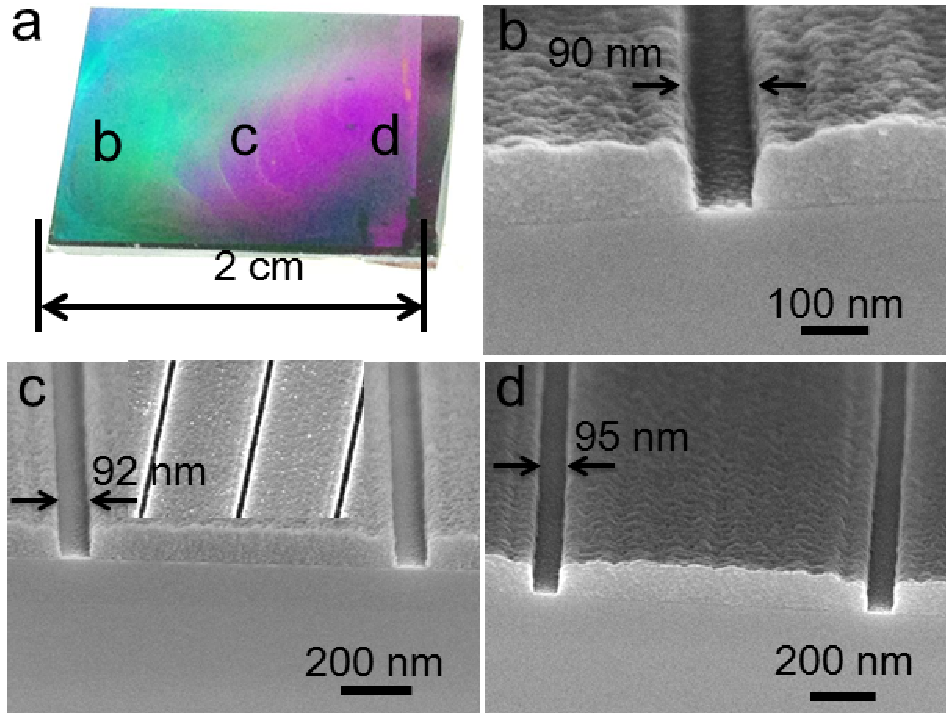

Figure S2. Study the uniformity of feature size for centimeter-scale nanopatterns. (a) Optical image of produced sub-wavelength positive photoresist nanopatterns across the areas of 2×1.5 cm^2. (b, c and d) SEM cross-sectional images of photoresist trenches with the trench widths of 90, 92 and 95 nm respectively, which were located at the left side, center part and right side of the centimeter-scale photoresist nanopatterns in (a).

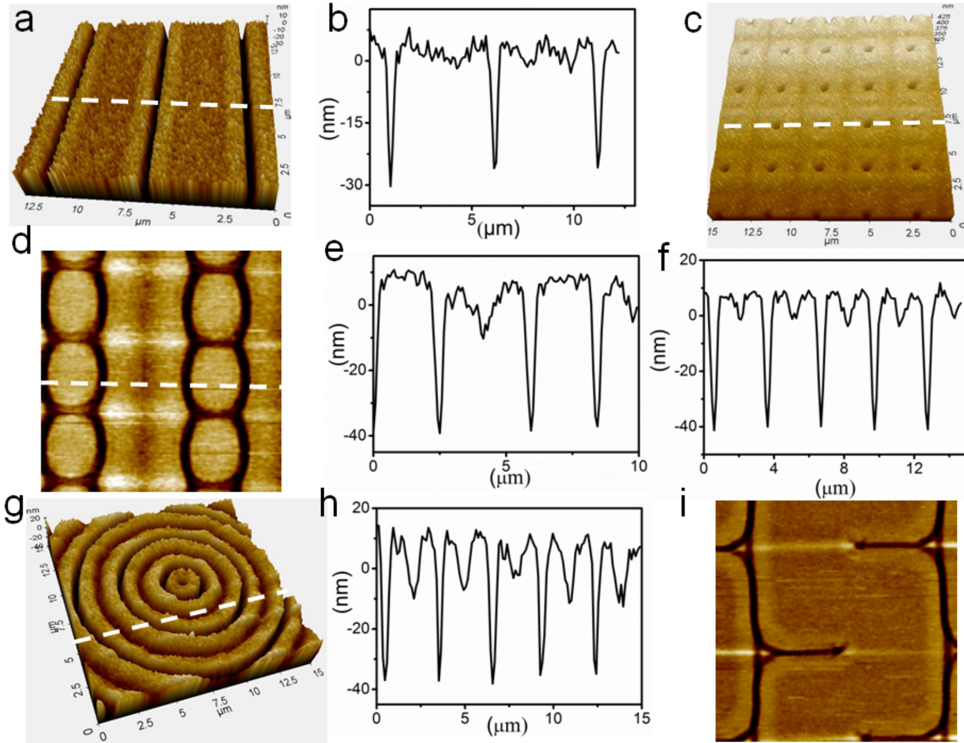

Figure S3. AFM topographical images of variously shaped positive photoresist nanopatterns with sub-wavelength feature size made by 20 nm Au coated V-shape PDMS tip array. (a) 3D AFM topographical image of positive photoresist straight trench nanopatterns. (b) AFM height profile of the white line across the nanopatterns in (a) indicating the nanoscale trench morphology of the nanopatterns. (c) 3D AFM topographical image of dot array. (d) AFM topographical image of nanostructures with ladder shape. (e and f) AFM height profiles of the white lines across the photoresist nanopatterns in (d) and (c) respectively. (g) 3D AFM topographical image of nanopatterns with circular shape. (h) AFM height profile of the white line in (g) across the photoresist nanopatterns. (i) AFM topographical image of nanopatterns with branch shape.

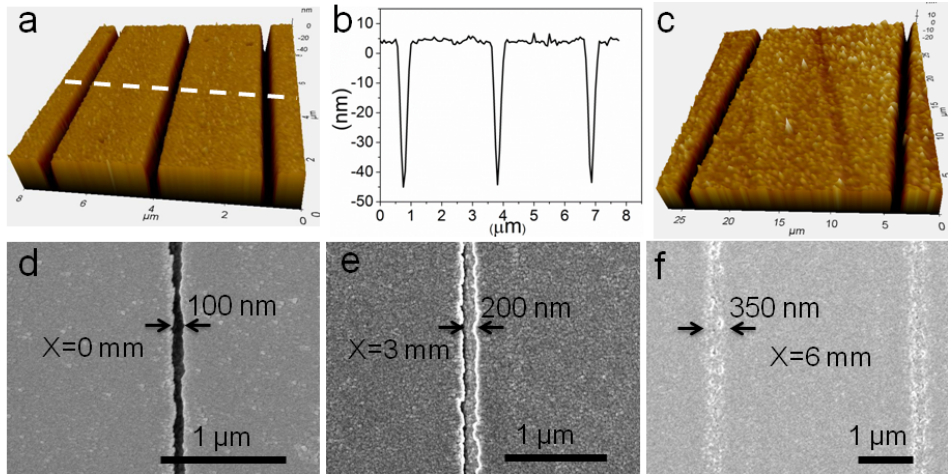

Figure S4. Photolithography with thick metal (60 nm Au) coated V-shape PDMS tips without apertures as photomasks. (a) and (c) 3D AFM topographical images of positive photoresist trench nanopatterns with the periodicities of 3 and 20 μm respectively. (b) AFM height profile of the white line across the nanopatterns in (a). The flat topography between two recessed positive photoresist trenches in (a-c) indicated that the photoresist below the flat backing parts between PDMS tips was nearly not exposed. (d, e and f) SEM images of produced positive photoresist trenches with the line widths of 100, 200 and 350 nm respectively, which were located at the positions with X coordinates of 0, 3 and 6 mm respectively on the same substrate. The above SEM images showed that the photoresist at the left side of the substrate surface (d) was fully exposed, while the photoresist at other places (e-f) was partially exposed. It demonstrated that the non-uniform feature sizes were produced by the non-sticky 60 nm Au coated PDMS tip array.

Besides sub-wavelength recessed nanopatterns produced on positive photoresist surface, this nanolithographic strategy also allowed for the production of large-area negative photoresist SU-8 nanopatterns with sub-wavelength feature dimension and adjustable feature height (Figure S5). The negative photoresist SU-8 2002 (MicroChem)

was pre-diluted with SU-8 2002 thinner at 20 % (v/v). The diluted SU-8 2002 (MicroChem) photoresist was spin coated on Si (100) wafers at 2000 rpm and 5000 rpm for 30 s to get 100 nm and 30 nm thick photoresist layers respectively. After baking of the photoresist-coated substrates on hot plate at 95 °C for 1 min, the samples were used for near-field photolithography by employing 20 nm Au coated PDMS pyramidal tip array as photomasks. The typical exposure time was 6 s. And the exposure energy of the halogen light source was 250 mW/cm^2. After exposure, the samples were post baked at 95 °C for 2 min, followed by the photoresist development in SU-8 developer for 5-10 s.

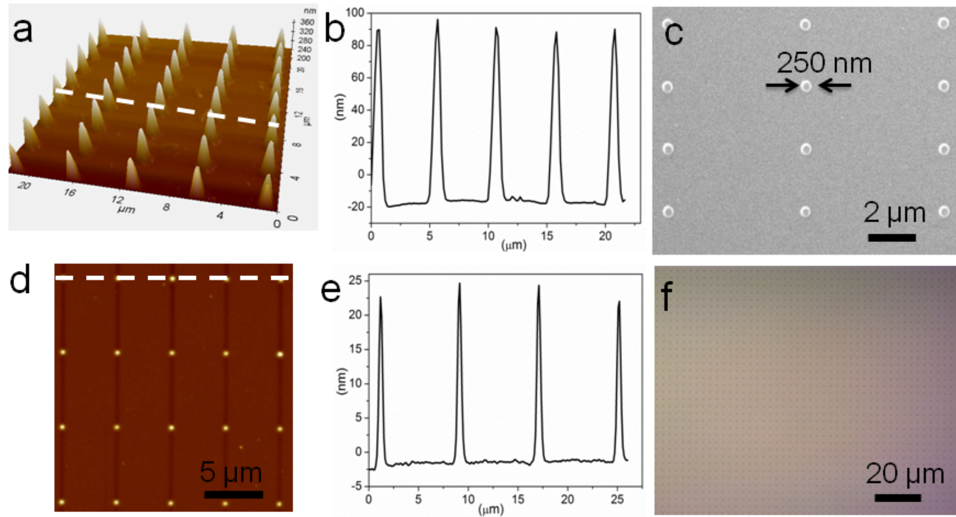

Figure S5. Fabrication of sub-wavelength raised negative photoresist SU-8 nanopatterns with variable feature height by this lithographic approach. (a) 3D AFM topographical image of SU-8 dot array. (b) AFM height profile of the white line across the photoresist nanopatterns in (a) indicating the feature height of 100 nm. (c) SEM image of SU-8 dot array in (a) showing the dot diameter of 250 nm. (d) AFM topographical image of SU-8 dot array. (e) AFM height profile of the white line across the photoresist nanopatterns in

(d) revealed the SU-8 dots with the height of 30 nm. (f) Optical image of large-area SU-8 dot array with sub-wavelength feature size.

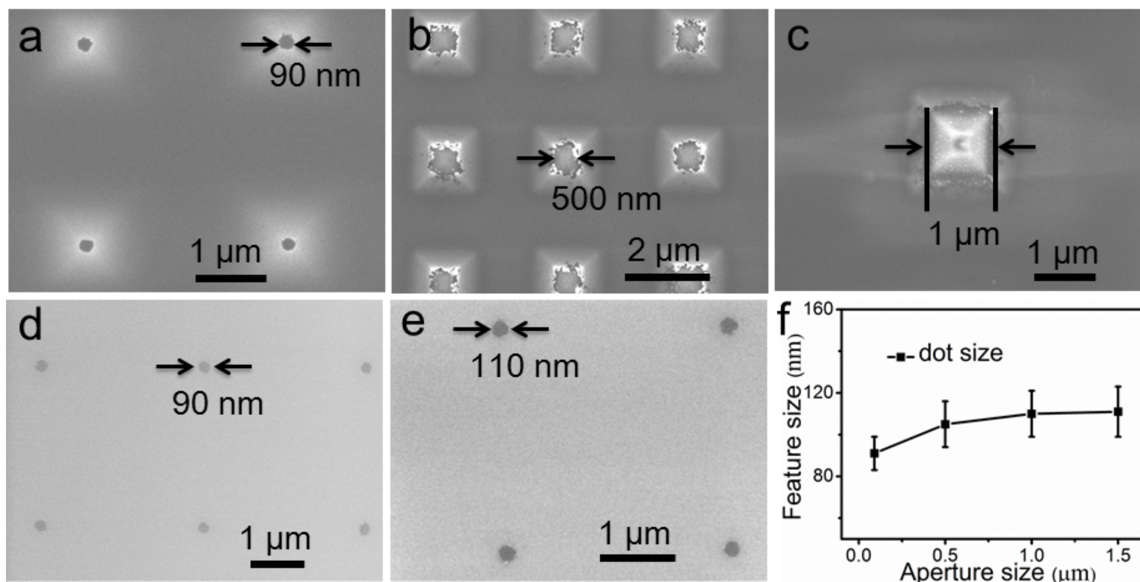

Figure S6. Study the effect of aperture size at metal-coated pyramidal PDMS tip apexes on the produced metal dot size. (a, b and c) SEM images of 60 nm Au coated PDMS pyramidal tips with the dot aperture sizes of 90 nm, 500 nm and 1 μm respectively. (d and e) SEM images of Cr dot arrays with the spot sizes of 90 and 110 nm respectively, which were created using the photomasks in (a) and (b) respectively. (f) Plot of produced Cr dot size as a function of aperture size at the end of metal-coated pyramidal PDMS tips.

Rotation angle (Degrees)	90	63	58	24	16	3
Ratio of length to width	1	1.5	2.5	6.25	8.33	50
Length of nanorod (nm)	90±11	120±17	300 ±31	750 ±55	1000 ±66	6000 ±87

Table S1. The dependence of the ratio of length to width and length of produced nanorod on the rotation angle of V-shape PDMS tip array in the second UV exposure.

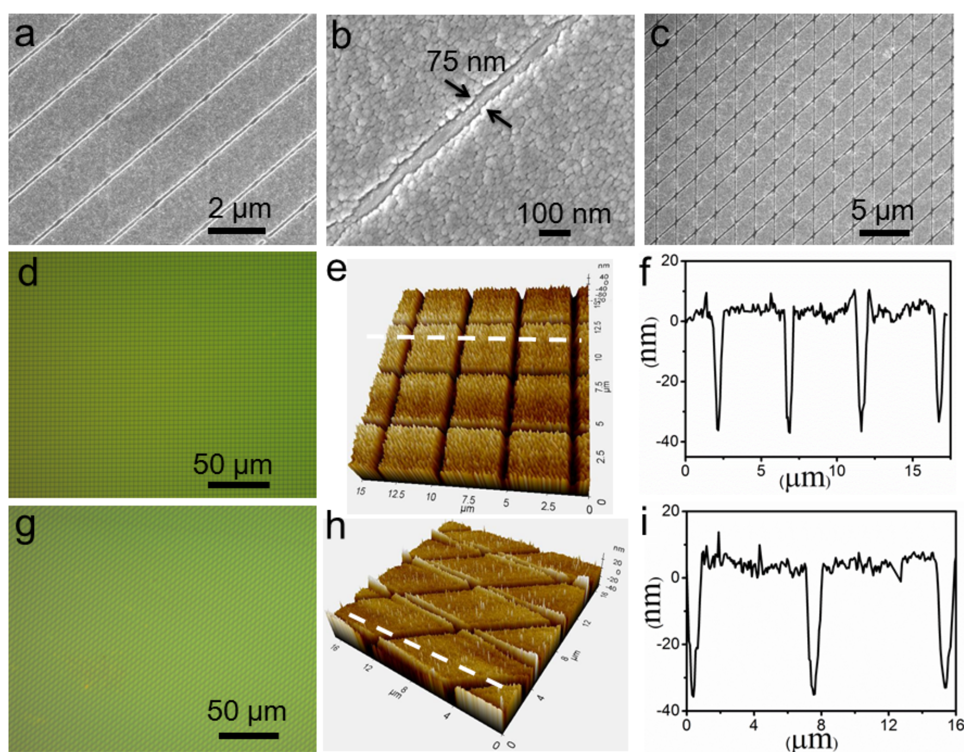

Figure S7. Large-area recessed positive photoresist nanopatterns with the shapes of grid and prism fabricated by rotating the photomasks for 90 and 45 degrees respectively in two exposures. (a) SEM image of photoresist lines produced by the first UV exposure. (b)

SEM image of one selected photoresist line in (a) with the line width of 75 nm. (c) SEM image of prismatic positive photoresist nanopatterns obtained after two exposures with rotation of photomask for 45 degrees in the second exposure. (d) and (e) Large-area optical image and AFM topographical image of positive photoresist grid nanopatterns respectively, which were fabricated by using the rotation angles of 90 degrees. (f) AFM height profile of the white line across the nanopatterns in (e). (g) and (h) Large-area optical image and AFM topographical image of prismatic photoresist nanopatterns respectively, which were achieved by using the rotation angles of 45 degrees. (i) AFM height profile of the white line across the nanopatterns in (h).

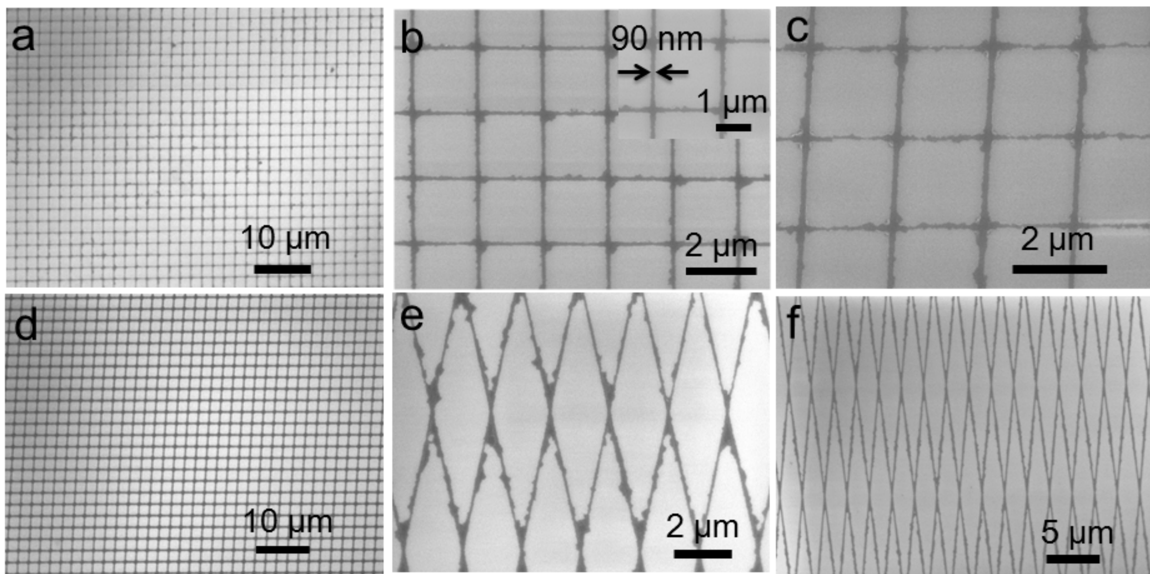

Figure S8. Fabrication of metal grid nanopatterns with programmable shapes and edge lengths by adjusting the rotation angles of PDMS tip photomasks in the second of two UV exposures. (a-b), (c-d), (e) and (f) SEM images of prismatic Cr nanostructures obtained by employing the rotation angles of 90, 86, 24 and 11 degrees respectively.